International Journal of Solids and Structures 311 (2025) 113253

Contents lists available at ScienceDirect

International Journal of Solids and Structures

journal homepage: www.elsevier.com/locate/ijsolstr

Deformation and stability of initially stressed hyperelastic plates

Soumya Mukherjee [a], Prashant Saxena [b,*]

[a] Department of Mechanical Engineering, Indian Institute of Technology Palakkad, Kanjikode, Kerala 678623, India
[b] Glasgow Computational Engineering Centre, James Watt School of Engineering, University of Glasgow, Glasgow G12 8LT, UK

ARTICLE INFO

Keywords:
Residual stress
Plate theory
Growth
Stability analysis

ABSTRACT

Initial/residual stress is inherent in nearly all natural and engineered structures. This paper presents a comprehensive theory for modelling residually stressed, growing plates. By constructing a two-dimensional representation of three-dimensional solid mechanics, we avoid any need for prior assumptions about deformation fields. This approach reformulates both the initial stress fields and deformation gradients in three-dimensional space through planar quantities, yielding a set of plate equations that govern their interactions. This framework enables modelling of various naturally and artificially generated planar structures with residual stress and growth, such as plant leaves and additively manufactured plates.

To explore the wrinkling instabilities that often arise in such structures, we derive a principal solution for an initially stressed, growing plate supported by Winkler foundations. We then apply linear perturbation to examine bifurcation phenomena, solving the resulting governing equations analytically and computationally. The numerical scheme is validated with analytical results and shows promise for solving more geometrically complex instability problems.

1. Introduction

This paper establishes a consistent finite deformation plate theory for initially stressed elastic solids, and unfolds the growth-induced instabilities in those initially stressed plates. Initial/ residual stress appears in biological systems due to growth, strain incompatibility, repairing, and remodelling. Almost all manufacturing processes, including welding (Salerno et al., 2018), machining (Wang et al., 2018a), additive manufacturing (Sun et al., 2021; Pidge and Kumar, 2020; Quelho de Macedo et al., 2019), introduce a residual stress. Growth and residual stress often introduce diverse surface textures and instabilities. We generalize the consistent theory of growing plates (Wang et al., 2018b) to include initially stressed non-linear elastic materials, and pursue a linear bifurcation analysis.

Initial stress influences the constitutive relation of a material (Johnson and Hoger, 1993, 1995; Saravanan, 2008; Shams et al., 2011; Merodio et al., 2013; Merodio and Ogden, 2016; Mukherjee and Ravindran, 2024; Mukherjee, 2022a; Mukherjee et al., 2022), alters its symmetry (Hoger, 1985; Rajagopal and Wineman, 2024; Mukherjee, 2024), affects the speed of wave propagation (Nam et al., 2016), and governs the static and dynamic properties of structures (Mukherjee and Mandal, 2021; Merodio et al., 2013; Merodio and Ogden, 2016).

Johnson and Hoger (1995, 1993) determined the response of an initially stressed Mooney–Rivlin materials — for which the associated stress-free reference is comprised of a Mooney–Rivlin solid. Saravanan (2011) developed the constitutive relation of a Blatz-Ko material model from an initially stressed reference. More models (Gower et al., 2015; Mukherjee, 2022b; Mukherjee and Ravindran, 2024; Mukherjee, 2024) have been developed for initially stressed reference configurations, using a virtual stress-free configuration. These models involve viscoelastcity (Mukherjee and Ravindran, 2024) as well as implicit elasticity (Mukherjee, 2024). Shams et al. (2011), Merodio et al. (2013), Merodio and Ogden (2016) developed a model for initially stressed materials where initial stress is used as the symmetry tensor representing the stress-induced anisotropy.

This paper develops a consistent plate theory for initially stressed soft materials. The goal of a plate theory is to reduce the dimension of a problem: to represent a three dimensional problem using two dimensions – to improve the analytical and computational efficiency. These structures are usually thinner. Hence, modelling them as a two-dimensional solid is physically justified. To this end, the three-dimensional displacement field, strain energy, and Cauchy stress are expressed in terms of displacement and other parameters on a given surface. The above goal has been accomplished by many small deformation plate theories like Kirchhoff, Mindlin Love (2013), and weakly non-linear theories like Föppl-von Kármán (Lewicka et al., 2011). Among the non-linear plate theories, we specially note (Hilgers and Pipkin, 1992b,a; Steigmann, 2007, 2013). Most small deformation plate

* Corresponding author.
E-mail addresses: s.mukherjee@iitpkd.ac.in (S. Mukherjee), prashant.saxena@glasgow.ac.uk (P. Saxena).

https://doi.org/10.1016/j.ijsolstr.2025.113253
Received 29 October 2024; Received in revised form 14 January 2025; Accepted 25 January 2025
Available online 6 February 2025

theories are based on apriori assumptions on the three-dimensional displacement field. Consequently, there are many plate theories of various orders, each of which applies to particular ranges of dimensions, materials, and deformation regimes. However, by extending the linear plate theory of Kienzler (2002) to non-linear deformations, Dai and Song (2014), Wang et al. (2016, 2018b, 2019) developed a consistent theory which does not presume any deformation field. Wang et al. (2018b) developed the theory for a growing plate. Mehta et al. (2021, 2022b) performed stability analysis of such plate structures using compound matrix methods. Our interest in this paper is to develop the consistent plate theory for initially stressed growing plates, and to perform stability analysis.

The numerical investigation of stability (Dorfmann and Haughton, 2006; Fu et al., 2020; Fu, 2007; Mehta et al., 2022a; Reddy and Saxena, 2018) is often performed using Compound matrix method (CMM) (Ng and Reid, 1985, 1980). It provides an efficient framework to solve various eigenvalue problems. We develop CMM to analyse stability in the context of this novel plate theory and it shows excellent agreements with our analytical solutions. This validation is necessary for its use in more complex boundary value problems based on this plate theory.

Developing the constitutive relations for initially stressed materials/references and employing them to solve various boundary and initial value problems, has been emerging as a popular field of research. However, there is no non-linear finite deformation plate theory developed for initially stressed elastic solids. The present work introduces a consistent plate theory for initially stressed, growing, thin-walled structures, and investigates its instability.

In thin structures, instabilities, including wrinkling, creasing, crumpling, etc., are often driven by initial/residual stress, and growth, which needs a thorough investigation. This initial stress is often unavoidable in most thin structures in nature. It may originate from processes such as growth, repairing, and remodelling. Furthermore, for analysis of thin, soft structures with residual stress, undergoing growth, a consistent plate theory has to be introduced, which is not available in the literature. Such a plate theory will be applicable to skin, leaves, and many thin structures used in engineering, to analyse the creation of bounteous shapes and surface textures in nature originated from growth and residual stress (Liang and Mahadevan, 2009, 2011). This paper develops an important consistent theory for initially stressed growing plates, which is employed to perform stability analysis in presence of growth.

The remaining part of this paper is organized as follows. Section 2 develops a two dimensional theory for initially stressed growing plates. The three dimensional kinematics is represented within a 2D plane, in Section 2.1. Section 2.2 develops the constitutive relations for the residually stressed growing plates. Section 2.3 represents the balance of linear momentum and the associated boundary conditions using two dimensions. Section 3 investigates the instabilities driven by initial stress and growth in a rectangular plate supported by Winkler foundations. The principal solution is determined in Section 3.1. The linear momentum balance equation is determined in Section 3.2. Section 3.3 determines the governing equation using a linear perturbation approach, which are solved analytically (Section 3.4) as well as numerically (Section 3.5) using CMM.

2. A two dimensional theory of growing initially stressed plates

In this section, we extend the consistent plate theory of Wang et al. (2018b, 2019), Dai and Song (2014) to include non-linear elastic plates with initial stress subject to growth.

Fig. 1 depicts the associated configurations, and the kinematic relations which interrelates them. The configuration $\mathfrak{R}$ undergoes growth (represented through a linear transformation $\boldsymbol{G}$) to generate the configuration $\mathfrak{R}_g$, which further undergoes the deformation of gradient $\boldsymbol{A}$ to appear at the current state $\mathfrak{C}$. Initial stress $\boldsymbol{\tau}$ is defined as a self-balancing stress in the configuration $\mathfrak{R}_g$, typically originated due to growth, or any other factor. To satisfy the balance of angular momentum, the initial stress tensor needs to be symmetric. If the internal stress does not involve a traction on the reference boundary, it is called a residual stress.

2.1. Two-dimensional kinematics

This section develops the kinematic relations for the initially stressed plate with growth in two dimensions.

A material point $\boldsymbol{X}$ in the undeformed plate $\mathfrak{R}$, can be expressed as $\boldsymbol{X} = (\boldsymbol{r}, Z)$, where $\boldsymbol{r}$ is the projection of the material position upon the bottom-surface of the plate, and Z is the through-thickness position.

A Taylor series expansion is used to express the three dimensional spatial location $\boldsymbol{x}$ (in the deformed configuration $\mathfrak{C}$) in terms of bottom surface quantities as follows,

$$\boldsymbol{x}(\boldsymbol{r}, Z) = \boldsymbol{x}^{(0)}(\boldsymbol{r}, 0) + Z\boldsymbol{x}^{(1)}(\boldsymbol{r}, 0) + \frac{Z^2}{2}\boldsymbol{x}^{(2)}(\boldsymbol{r}, 0) + \cdots, \tag{2.1}$$

where $\boldsymbol{x}^{(i)} = \frac{\partial^i \boldsymbol{x}}{\partial Z^i}$, and all quantities at the right hand side are defined at the bottom surface ($Z = 0$). Differentiating (2.1), with respect to the material position $\boldsymbol{X} = (\boldsymbol{r}, Z)$, the deformation gradient $\frac{\mathrm{d}\boldsymbol{x}}{\mathrm{d}\boldsymbol{X}}$ is expanded as,

$$\boldsymbol{F} = \boldsymbol{F}^{(0)}(\boldsymbol{r}, 0) + Z\boldsymbol{F}^{(1)}(\boldsymbol{r}, 0) + \frac{Z^2}{2}\boldsymbol{F}^{(2)}(\boldsymbol{r}, 0) + \cdots, \tag{2.2}$$

where $\boldsymbol{F}^{(n)}$ is decomposed into the in-plane and out-of-plane components (obtained by differentiation with respect to Z) as follows:

$$\boldsymbol{F}^{(n)} = \boldsymbol{\nabla}\boldsymbol{x}^{(n)} + \boldsymbol{x}^{(n+1)} \otimes \boldsymbol{k}, \tag{2.3}$$

where $\boldsymbol{\nabla}$ denotes the in-plane differentiation operator, and $\boldsymbol{k} = \frac{\partial \boldsymbol{X}}{\partial Z}$. Fig. 1 explains the multiplicative decomposition of deformation gradient $\boldsymbol{F}$ into the gradient $\boldsymbol{A}$ and the growth tensor $\boldsymbol{G}$. We expand the Growth tensors $\boldsymbol{G}$, $J_g\boldsymbol{G}^{-1}$, and the gradient $\boldsymbol{A} = \boldsymbol{F}\boldsymbol{G}^{-1}$ around the bottom surface ($Z = 0$) as,

$$\boldsymbol{G}^{-T} = \sum_n \frac{Z^n}{n!}\boldsymbol{G}^{(n)}, \qquad J_g\boldsymbol{G}^{-1} = \sum_n \frac{Z^n}{n!}\hat{\boldsymbol{G}}^{(n)}, \qquad \boldsymbol{A} = \sum_n \frac{Z^n}{n!}\boldsymbol{A}^{(n)}. \tag{2.4}$$

The deformation gradient $\boldsymbol{A}$, (measured from the reference $\mathfrak{R}_g$) is expressed using the following multiplicative decomposition

$$\boldsymbol{A} = \boldsymbol{F}\boldsymbol{G}^{-1} = \sum_{r=0}^{n} \frac{Z^n}{r!\,(n-r)!}\boldsymbol{F}^{(r)}\boldsymbol{G}^{(n-r)}. \tag{2.5}$$

Equating the coefficients of Z^n in (2.4c) and (2.5), we obtain,

$$\boldsymbol{A}^{(n)} = \sum_{r=0}^{n} C_r^n \boldsymbol{F}^{(r)}\boldsymbol{G}^{(n-r)}, \tag{2.6}$$

where $C_r^n = \frac{n!}{r!\,(n-r)!}$. It should be noted that the first two terms in the Taylor series expansion for $\boldsymbol{A}$ are obtained from (2.6) as

$$\boldsymbol{A}^{(0)} = \boldsymbol{F}^{(0)}\boldsymbol{G}^{(0)}, \qquad \boldsymbol{A}^{(1)} = \boldsymbol{F}^{(0)}\boldsymbol{G}^{(1)} + \boldsymbol{F}^{(1)}\boldsymbol{G}^{(0)}. \tag{2.7}$$

Upon substitution of (2.3) into (2.6), $\boldsymbol{A}^{(n)}$ is represented as

$$\boldsymbol{A}^{(n)} = \boldsymbol{\nabla}\boldsymbol{x}^{(n)}\boldsymbol{G}^{(0)} + \boldsymbol{x}^{(n+1)} \otimes \left[\boldsymbol{G}^{(0)}\right]^T \boldsymbol{k} + \sum_{r=0}^{n-1} C_r^n \boldsymbol{F}^{(r)}\boldsymbol{G}^{(n-r)}. \tag{2.8}$$

2.2. Constitutive relations in two-dimensions

In a three dimensional space, the first Piola Kirchhoff stress can be determined from a hyperelastic framework as,

$$\boldsymbol{P} = J_g\left(\frac{\partial \phi_0(\boldsymbol{A}, \boldsymbol{\tau})}{\partial \boldsymbol{A}} - p\frac{\partial R_0}{\partial \boldsymbol{A}}\right)\boldsymbol{G}^{-T}, \tag{2.9}$$

where $R_0(\boldsymbol{A}) = \det\boldsymbol{A} - 1 = 0$, and $\phi_0(\boldsymbol{A}, \boldsymbol{\tau})$ is the strain energy density for initially stressed materials.

Note here that $R_0 = \det\boldsymbol{A} - 1 = 0$ is used to enforce the constraint of incompressibility. The same form of R_0 can be used in the presence of residual stress. On the other hand, for compressible materials, R_0 depends on the initial/residual stress in general since it introduces

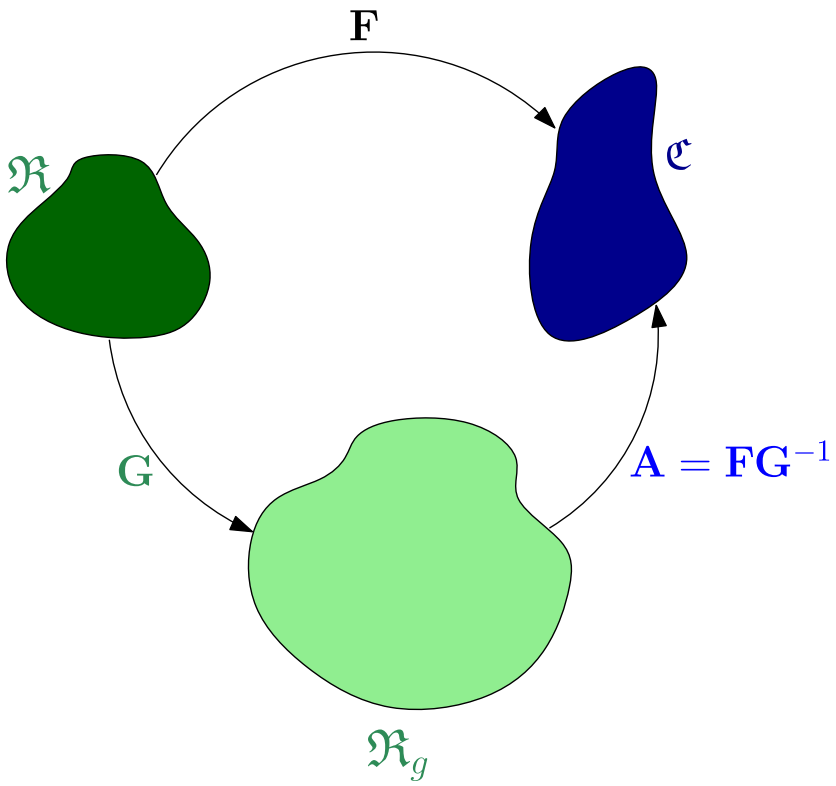

Fig. 1. The muliplicative decomposition of deformation gradient $\boldsymbol{F}$ from $\mathfrak{R}$ to $\mathfrak{C}$. The reference $\mathfrak{R}$ undergoes growth $\boldsymbol{G}$ create the configuration $\mathfrak{R}_g$. The configuration $\mathfrak{R}_g$ further undergoes a deformation with gradient $\boldsymbol{A}$ to generate $\mathfrak{C}$.

volumetric initial strain in the associated stress-free body (Mukherjee et al., 2022).

The above three-dimensional stress field can be expanded around the bottom surface as

$$\boldsymbol{P} = \sum_n \frac{Z^n}{n!}\boldsymbol{P}^{(n)}, \tag{2.10}$$

where $\boldsymbol{P}^{(n)} = \frac{\partial^n \boldsymbol{P}}{\partial Z^n}\Big|_{Z=0}$. We also represent the three dimensional initial stress-field using the quantities at the bottom-surface, as follows,

$$\boldsymbol{\tau} = \sum_n \frac{Z^n}{n!}\boldsymbol{\tau}^{(n)}, \tag{2.11}$$

where $\boldsymbol{\tau}^{(n)} = \frac{\partial^n \boldsymbol{\tau}}{\partial Z^n}\Big|_{Z=0}$. The Taylor series expansion of $\frac{\partial \phi_0}{\partial \boldsymbol{A}}$, p, and $\frac{\partial R_0}{\partial \boldsymbol{A}}$ can be used to expand the Piola–Kirchhoff stress (2.9) as follows,

$$\begin{aligned}\boldsymbol{P} = &\left(\sum_s \frac{Z^s}{s!}\hat{\boldsymbol{G}}^{(s)}\right)\left(\mathbb{A}^{(0)} + \mathbb{A}^{(1)}\left[\sum_{m_1=1} \frac{Z^{m_1}}{m_1!}\boldsymbol{A}^{(m_1)}\right] + \cdots\right)\\ &+ \left(\sum_s \frac{Z^s}{s!}\hat{\boldsymbol{G}}^{(s)}\right)\left(\mathbb{B}^{(0,1)}\left[\sum_{r_1=1} \frac{Z^{r_1}}{r_1!}\boldsymbol{\tau}^{(r_1)}\right] + \cdots\right)\\ &- \left(\sum_s \frac{Z^s}{s!}\hat{\boldsymbol{G}}^{(s)}\right)\left(\sum_q \frac{Z^q}{q!}p^{(q)}\right)\left(\mathbb{R}^{(0)} + \mathbb{R}^{(1)}\left[\sum_{m_1=1} \frac{Z^{m_1}}{m_1!}\boldsymbol{A}^{(m_1)}\right] + \cdots\right),\end{aligned} \tag{2.12}$$

where $\mathbb{A}^{(k)} = \frac{\partial^{k+1}\phi_0}{\partial \boldsymbol{A}^{k+1}}$, $\mathbb{B}^{(k,m)} = \frac{\partial^{k+m+1}\phi_0}{\partial \boldsymbol{A}^{k+1}\partial \boldsymbol{\tau}^m}$, $\mathbb{R}^{(k)} = \frac{\partial^{k+1} R}{\partial \boldsymbol{A}^{k+1}}$, $\hat{\boldsymbol{G}}^{(s)}$ is defined in Eq. (2.4b). All these tensors are functionally dependent on the bottom surface quantities such as $\boldsymbol{A}^{(0)}$, $\boldsymbol{\tau}^{(0)}$ … The tensors $\mathbb{A}^{(k)}$, $\mathbb{B}^{(k,m)}$, and $\mathbb{R}^{(k)}$ are of the orders $(2k+2)$, $(2k+2m+2)$, and $(2k+2)$, respectively, and are detailed as

$$\mathbb{A}^{(1)}_{ijkl} = \frac{\partial^2 \phi_0}{\partial A_{ij}\partial A_{kl}}, \quad \left\{\mathbb{A}^{(2)}\left[\boldsymbol{A}^{(1)}, \boldsymbol{A}^{(2)}\right]\right\}_{ij} = \mathbb{A}^{(2)}_{ijklmn}\boldsymbol{A}^{(1)}_{kl}\boldsymbol{A}^{(2)}_{mn}, \ldots$$

Comparing and equating the coefficients of Z^n in (2.10b) and (2.12), we obtain

$$\begin{aligned}\boldsymbol{P}^{(n)} = &\sum_{\substack{s=0,k=0,m_i=1,\\ \sum m_i = n-s}}^{n} \frac{n!}{s!\,m_1!\,m_2!\,\ldots,m_k!}\hat{\boldsymbol{G}}^{(s)}\mathbb{A}^{(k)}\left[\boldsymbol{A}^{(m_1)}, \boldsymbol{A}^{(m_2)}, \ldots, \boldsymbol{A}^{(m_k)}\right]\\ &+ \sum_{\substack{s=0,k=0,m_i=1\\ \sum m_i + \sum p_i = n-s}}^{n} \frac{n!}{s!\,m_1!\,\ldots,m_k!\,p_1!\,\ldots\,p_r!}\hat{\boldsymbol{G}}^{(s)}\mathbb{B}^{(k,r)}\left[\boldsymbol{A}^{(m_1)}\ldots,\boldsymbol{A}^{(m_k)}, \boldsymbol{\tau}^{(p_1)}\ldots,\boldsymbol{\tau}^{(p_r)}\right]\\ &- \sum_{\substack{s=0,q=0,k=0,m_i=1\\ \sum m_i = n-s-q}}^{n} \frac{n!}{s!\,q!\,m_1!\,m_2!\,\ldots,m_k!}\hat{\boldsymbol{G}}^{(s)}p^{(q)}\mathbb{R}^{(k)}\left[\boldsymbol{A}^{(m_1)}, \boldsymbol{A}^{(m_2)}, \ldots, \boldsymbol{A}^{(m_k)}\right].\end{aligned} \tag{2.13}$$

For $n = 0$ and 1, $\boldsymbol{P}^{(n)}$ in Eq. (2.13) is expressed as

$$\boldsymbol{P}^{(0)} = \hat{\boldsymbol{G}}^{(0)}\mathbb{A}^{(0)} - \hat{\boldsymbol{G}}^{(0)}p^{(0)}\mathbb{R}^{(0)} \tag{2.14}$$

$$\boldsymbol{P}^{(1)} = \hat{\boldsymbol{G}}^{(1)}\mathbb{A}^{(0)} + \hat{\boldsymbol{G}}^{(0)}\mathbb{A}^{(1)} + \hat{\boldsymbol{G}}^{(0)}\mathbb{B}^{(0,1)}\left[\boldsymbol{\tau}^{(1)}\right] - \hat{\boldsymbol{G}}^{(0)}p^{(0)}\mathbb{R}^{(1)}\left[\boldsymbol{A}^{(1)}\right] \tag{2.15}$$

$$- \hat{\boldsymbol{G}}^{(1)}p^{(0)}\mathbb{R}^{(0)} - \hat{\boldsymbol{G}}^{(0)}p^{(1)}\mathbb{R}^{(0)}. \tag{2.16}$$

The initial stress $\boldsymbol{\tau}^{(0)}$ at the bottom surface appears in these expressions through $\mathbb{A}^{(n)}$ and $\mathbb{B}^{(p,q)}$.

We can also use Eq. (2.8) to rewrite the constitutive relation (2.13) for $\boldsymbol{P}^{(n+1)}$ as

$$\boldsymbol{P}^{(n+1)} = \hat{\boldsymbol{G}}^{(0)}\left(\mathbb{A}^{(1)} - p^{(0)}\mathbb{R}^{(1)}\right)\left[\boldsymbol{x}^{(n+2)} \otimes \left[\boldsymbol{G}^{(0)}\right]^T \boldsymbol{k}\right] - p^{(n+1)}\hat{\boldsymbol{G}}^{(0)}\mathbb{R}^{(0)} + \bar{\boldsymbol{P}}^{(n+1)}, \tag{2.17}$$

where $\bar{\boldsymbol{P}}^{(n+1)}$ represents the additional terms in $\boldsymbol{P}^{(n+1)}$.

We further interrelate $\mathbb{R}^{(k)}$ using the Taylor series expansion of $R(\boldsymbol{A}) = \det \boldsymbol{A}$ as

$$R(\boldsymbol{A}) = R\left(\boldsymbol{A}^{(0)}\right) + \mathbb{R}^{(0)}\left(\boldsymbol{A}^{(0)}\right)\left[\sum_{n=1} \frac{Z^n}{n!}\boldsymbol{A}^{(n)}\right] + \cdots = 1,$$

which is equivalent to writing

$$\sum_{i=0} \frac{1}{i!}\mathbb{R}^{(i-1)}\left(\boldsymbol{A}^{(0)}\right)\left[\sum_{n_1=1} \frac{Z^{n_1}}{n_1}\boldsymbol{A}^{(n_1)}, \ldots, \sum_{n_i=1} \frac{Z^{n_i}}{n_i}\boldsymbol{A}^{(n_i)}\right] = 0, \tag{2.18}$$

equating $R\left(\boldsymbol{A}^{(0)}\right)$ with 1. Vanishing the coefficients of Z^p (for $p>0$) in (2.18), we obtain

$$\sum_{\substack{k=0,n_i=1\\ \sum n_i=p}}^{k=p} \frac{1}{(k+1)!\,n_1!\,n_2!\,\ldots,n_k!}\mathbb{R}^{(k)}\left[\boldsymbol{A}^{(n_1)},\boldsymbol{A}^{(n_2)},\ldots,\boldsymbol{A}^{(n_k)}\right]=0. \tag{2.19}$$

In this section, we have expressed the constitutive relations using only two dimensions (on the bottom surface) of the continua. The kinematic relations such as (2.19) are useful to establish the balance of linear momentum in the next section.

2.3. The balance of linear momentum and the boundary conditions in 2D

Using the in-plane and out-of-plane projection of divergence, the balance of linear momentum Div $\boldsymbol{P}=0$ is represented as

$$\boldsymbol{\nabla}\cdot\boldsymbol{P}^{(n)}+\left(\boldsymbol{P}^{(n+1)}\right)^T\boldsymbol{k}=0,\quad \forall n\geq 0. \tag{2.20}$$

We substitute Eq. (2.17) into the linear momentum balance Eq. (2.20) above, to obtain

$$\mathfrak{B}\boldsymbol{x}^{(n+2)}+\boldsymbol{f}^{(n+2)}-p^{(n+1)}\left[\hat{\boldsymbol{G}}^{(0)}\mathbb{R}^{(0)}\right]^T\boldsymbol{k}=0, \tag{2.21}$$

where

$$\mathfrak{B}_{ij}=\left(\mathbb{A}^{(1)}_{\alpha i\beta j}-p^{(0)}\mathbb{R}^{(1)}_{\alpha i\beta j}\right)\left(\left[\hat{\boldsymbol{G}}^{(0)}\right]^T\boldsymbol{k}\right)_\alpha\left(\left[\boldsymbol{G}^{(0)}\right]^T\boldsymbol{k}\right)_\beta, \tag{2.22}$$

$$\boldsymbol{f}^{(n+2)}=\boldsymbol{\nabla}\cdot\boldsymbol{P}^{(n)}+\left(\bar{\boldsymbol{P}}^{(n+1)}\right)^T\boldsymbol{k}. \tag{2.23}$$

Eq. (2.21) can be easily inverted to obtain a solution for $\boldsymbol{x}^{(n+2)}$ as

$$\boldsymbol{x}^{(n+2)}=-\mathfrak{B}^{-1}\boldsymbol{f}^{(n+2)}+p^{(n+1)}\mathfrak{B}^{-1}\left[\hat{\boldsymbol{G}}^{(0)}\mathbb{R}^{(0)}\right]^T\boldsymbol{k}, \tag{2.24}$$

It is noted that the coefficient of Z^{n+1} in (2.19) can be rewritten as

$$\frac{1}{(n+1)!}\mathbb{R}^{(0)}\left[\boldsymbol{x}^{(n+2)}\otimes\left[\boldsymbol{G}^{(0)}\right]^T\boldsymbol{k}+\boldsymbol{\nabla}\boldsymbol{x}^{(n+1)}\boldsymbol{G}^{(0)}+\sum_{r=0}^{n-1}C^n_r\boldsymbol{F}^{(r)}\boldsymbol{G}^{(n-r)}\right]+\cdots=0 \tag{2.25}$$

where the terms within square bracket is recognized as $\boldsymbol{A}^{(n+1)}$ from Eq. (2.8). Substituting Eq. (2.24) into (2.25), we can form a linear algebraic equation. The resulting equation and Eq. (2.24) need to be solved iteratively to obtain $p^{(n+1)}$ and $\boldsymbol{x}^{(n+2)}$.

In (2.20), the balance of force is expressed in terms of the first Piola–Kirchhoff stress. The initial stress (defined as the stress in the reference configuration) should also satisfy the balance Eq. (2.20) as

$$\boldsymbol{\nabla}.\boldsymbol{\tau}^{(n)}+\boldsymbol{\tau}^{(n+1)}\boldsymbol{k}=0,\quad \forall n\geq 0. \tag{2.26}$$

The traction on the top and bottom surfaces of the plate are given by $\boldsymbol{q}^+$ and $\boldsymbol{q}^-$ respectively. Consequently, the Neumann boundary condition at the bottom surface of the plate (Wang et al., 2019) is given by

$$(\boldsymbol{P})^T\boldsymbol{k}\Big|_{Z=0}=\left(\boldsymbol{P}^{(0)}\right)^T\boldsymbol{k}=\boldsymbol{q}^- \tag{2.27}$$

On the other hand, the boundary condition on the top surface is given by,

$$(\boldsymbol{P})^T\boldsymbol{k}\Big|_{Z=2h}=\sum_{n=0}\frac{(2h)^n}{n!}\left(\boldsymbol{P}^{(n)}\right)^T\boldsymbol{k}=\boldsymbol{q}^+. \tag{2.28}$$

Subtracting Eq. (2.27) from Eq. (2.28), and substituting $\left(\boldsymbol{P}^{(n+1)}\right)^T\boldsymbol{k}=\boldsymbol{\nabla}\cdot\boldsymbol{P}^{(n)}$ (see (2.20)), we obtain

$$\sum_{n=0}\frac{(2h)^n}{n!}\boldsymbol{\nabla}\cdot\boldsymbol{P}^{(n)}=\boldsymbol{q}^+-\boldsymbol{q}^-. \tag{2.29}$$

Note that a residual stress field $\boldsymbol{\tau}$, which does not introduce any boundary traction, will similarly satisfy a condition

$$\sum_{n=0}\frac{(2h)^n}{n!}\boldsymbol{\nabla}\cdot\boldsymbol{\tau}^{(n)}=\boldsymbol{0}. \tag{2.30}$$

Eqs. (2.29) and (2.30) represent the balance of linear momentum in the deformed and the undeformed plate in a reduced two dimensional space.

3. The deformation and instabilities of a growing, initially stressed, rectangular plate

This section details the governing equations and investigates the stability of a growing rectangular plate subject to an initial stress, analytically and numerically. The plate lies between $-1<X<1$ with thickness $2h$ along the Z direction. The top surface of the plate is supported by Winkler foundation (Wang et al., 2018b) as shown schematically in Fig. 2.

The constant growth tensor is chosen as

$$\mathbf{G}=\mathrm{diag}\,(\lambda,1,1). \tag{3.1}$$

Using (2.1), the spatial co-ordinates of a point can be expressed as,

$$x=\sum_n\frac{Z^n}{n!}x^{(n)},\qquad y=Y,\qquad z=\sum_n\frac{Z^n}{n!}z^{(n)}. \tag{3.2}$$

The deformation gradient at the bottom-surface is given by $\boldsymbol{F}=\sum_n\frac{Z^n}{n!}\boldsymbol{F}^{(n)}$, where

$$\boldsymbol{F}^{(n)}=\begin{bmatrix}x^{(n)\prime} & 0 & x^{(n+1)}\\ 0 & 1 & 0\\ z^{(n)\prime} & 0 & z^{(n+1)}\end{bmatrix} \tag{3.3}$$

using (2.3). We consider a uni-axial initial stress component τ_{XX}. This initial stress component is supported by traction on the boundaries normal to the X direction. We further consider a constant initial stress component τ_{XX} through thickness, such that $\tau^{(1)}_{XX}=\tau^{(2)}_{XX}=\cdots=\tau^{(n)}_{XX}=0$ for $n>0$.

The boundary conditions at the traction-free bottom surface $Z=0$, and at the top surface supported by the Winkler foundation are represented by

$$q^-_i=0, \qquad \forall i\in\{1,2,3\} \tag{3.4}$$

$$q^+_i=0, \qquad \forall i\in\{1,2\} \tag{3.5}$$

$$q^+_3(X)=-\alpha_1\mu\lambda\left[z(x,2h)-2h\right], \tag{3.6}$$

where α_1 is a known constant. The influence of initial stress is probed through a constitutive relation for which

$$\phi_0(\boldsymbol{A},\boldsymbol{\tau})=\mu\,\mathrm{tr}\left(\boldsymbol{A}^T\boldsymbol{A}\right)+\boldsymbol{\tau}:\left[\boldsymbol{A}^T\boldsymbol{A}\right] \tag{3.7}$$

and $R_0=\det\boldsymbol{A}-1$ in Eq. (2.9). This constitutive relation was proposed by Shams et al. (2011) for residually stressed materials without considering growth. Other constitutive relations for initially stressed isotropic elastic materials can be found in Johnson and Hoger (1993, 1995), Saravanan (2008), Gower et al. (2015), Mukherjee (2022a), which use a virtual stress-free configuration. The present constitutive relation is used in Section 3.1 to obtain the principal solution.

3.1. Principal solutions for growing initially stressed plates

In this section, we determine the principal solution for growing initially stressed plates, which is later subject to perturbation to perform stability analysis.

For the constitutive relation (3.7), the nth order term $\boldsymbol{P}^{(n)}$ of the first Piola–Kirchhoff stress is obtained from Eq. (2.13) as

$$\boldsymbol{P}^{(n)}=\lambda\left(2\mu\boldsymbol{F}^{(n)}\mathbf{G}^{-1}+\boldsymbol{F}^{(n)}\mathbf{G}^{-1}\boldsymbol{\tau}^{(n)}-p^{(n)}\mathbb{R}^{(0)}-p^{(n-1)}\mathbb{R}^{(1)}\left[\boldsymbol{F}^{(1)}\mathbf{G}^{-1}\right]-\cdots\right)\mathbf{G}^{-T} \tag{3.8}$$

The above constitutive relation contains $\boldsymbol{F}^{(n)}$ which involves many higher order terms, $x^{(n)}$, $z^{(n)}$, $p^{(n-1)}$ for $n\geq 0$, as described in (3.3). We express all the higher order terms as functions of $x^{(0)}$ and $z^{(0)}$ iteratively, using the approach of Section 2.3, as follows.

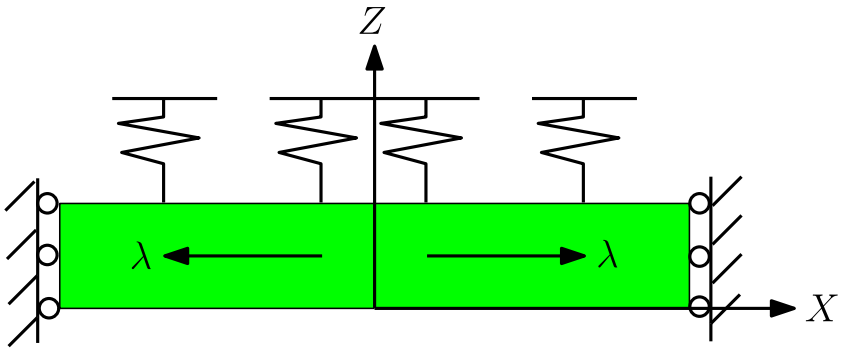

Fig. 2. Growing initially stressed plate (with non-zero $\tau^{(0)}_{XX}$ component) supported by a Winkler foundation at the top surface.

First, to determine $x^{(1)}$, $z^{(1)}$, in terms of $x^{(0)}$, $z^{(0)}$, and $p^{(0)}$, we substitute the constitutive relation (3.8) (for $n = 0$) into the boundary condition (2.27). For $n \geq 0$, $x^{(n+2)}$, $z^{(n+2)}$ are expressed in terms of $x^{(0)}$, $z^{(0)}$, $p^{(0)}$, $p^{(1)}, \dots, p^{(n+1)}$ by iteratively using (2.24). All unknown $p^{(n)}$ are obtained in terms of $x^{(0)}$ and $z^{(0)}$ using the following set of equations, obtained from Eq. (2.19).

$$\boldsymbol{R}\left(\boldsymbol{A}_0\right) = 1 \tag{3.9}$$

$$\mathbb{R}^{(0)}\left[\boldsymbol{A}^{(1)}\right] = 0 \tag{3.10}$$

$$\mathbb{R}^{(0)}\left[\boldsymbol{A}^{(2)}\right] + \mathbb{R}^{(1)}\left[\boldsymbol{A}^{(1)}, \boldsymbol{A}^{(1)}\right] = 0 \tag{3.11}$$

$$\mathbb{R}^{(0)}\left[\boldsymbol{A}^{(3)}\right] + 3\mathbb{R}^{(1)}\left[\boldsymbol{A}^{(1)}, \boldsymbol{A}^{(2)}\right] + \mathbb{R}^{(2)}\left[\boldsymbol{A}^{(1)}, \boldsymbol{A}^{(1)}, \boldsymbol{A}^{(1)}\right] = 0 \tag{3.12}$$

...

The above methodology is demonstrated in Appendix through explicit determination of some $x^{(n)}$, $z^{(n)}$, and $p^{(n)}$ for the chosen constitutive relation (3.7), (3.8).

In presence of growth and a uniform initial stress field $\boldsymbol{\tau}^{(0)}$, a deformation field

$$x^{(0)} = X \qquad z^{(0)} = c_0 \qquad \dots \qquad z^{(m)} = c_m, \tag{3.13}$$

is predicted, which is homogeneous along the X direction. Substituting (3.13a) and (3.13b) respectively into (A.4)–(A.12), we obtain

$$z^{(1)} = c_1 = \lambda \qquad z^{(m)} = c_m = 0, \quad \text{for } m > 1. \tag{3.14}$$

In addition, $z^{(0)} = -2h\,(\lambda - 1)$ ensures that

$$z\Big|_{Z=2h} = z^{(0)} + 2hz^{(1)} = 2h,$$

such that the flexible Winkler foundation does not apply any traction at the top surface.

Hence, the principal solution for this case, is given by,

$$x^{(0)} = X \qquad z^{(0)} = -2h\,(\lambda - 1)\,. \tag{3.15}$$

It can be checked that this principal solution satisfies the boundary conditions:

$$\boldsymbol{x}\Big|_{X=-1} = 0 \qquad \boldsymbol{x}\Big|_{X=1} = 0 \tag{3.16}$$

$$P_{13}\Big|_{X=-1} = 0 \qquad P_{13}\Big|_{X=1} = 0. \tag{3.17}$$

3.2. The balance equations for rectangular plates

As we introduce perturbations to the principal solution (3.15), the resulting solutions will be inhomogeneous in X. To determine these inhomogeneous terms, a complete description of the balance equation is necessary, which we obtain in this section.

Substituting the constitutive relation (3.8) into the balance of linear momentum in 2D, Eq. (2.29) (for $n = 0, 1, 2$), we obtain

$$\begin{aligned}
&\frac{2\mu + \tau^{(0)}_{XX}}{\lambda} x^{(0)\prime\prime} + 2\mu\lambda x^{(1)} + p^{(0)} z^{(0)\prime} - p^{(0)} z^{(1)\prime} \\
&- z^{(1)} p^{(0)\prime} h\left(p^{(0)} z^{(1)\prime} + p^{(1)} z^{(0)\prime} - p^{(0)} z^{(2)\prime} - p^{(1)} z^{(1)\prime}\right. \\
&\left. - z^{(1)} p^{(1)\prime} - z^{(2)} p^{(0)\prime} + 2\mu\lambda x^{(2)}\right) + \frac{h}{\lambda}\left[\left(2\mu + \tau^{(0)}_{XX}\right) x^{(1)\prime\prime} + \tau^{(1)}_{XX} x^{(0)\prime\prime}\right] \\
&+ \frac{h^2}{2}\left(p^{(0)} z^{(2)\prime} + 2p^{(1)} z^{(1)\prime} + p^{(2)} z^{(0)\prime} + 2\mu\lambda x^{(3)}\right) \\
&- \frac{h^2}{2}\left(p^{(0)} z^{(3)\prime} + 2p^{(1)} z^{(2)\prime} + p^{(2)} z^{(1)\prime} + z^{(1)} p^{(2)\prime} + 2z^{(2)} p^{(1)\prime} + z^{(3)} p^{(0)\prime}\right) \\
&+ \frac{h^2}{2\lambda}\left[\left(2\mu + \tau^{(0)}_{XX}\right) x^{(2)\prime\prime} + 2\tau^{(1)}_{XX} x^{(2)\prime\prime}\right] = q_1^+ - q_1^-,
\end{aligned} \tag{3.18}$$

$$\begin{aligned}
&\frac{2\mu + \tau^{(0)}_{XX}}{\lambda} z^{(0)\prime\prime} + 2\mu\lambda z^{(1)} - p^{(0)} x^{(0)\prime} + p^{(0)} x^{(1)\prime} + x^{(1)} p^{(0)\prime} \\
&+ h\left(p^{(0)} x^{(2)\prime} - p^{(1)} x^{(0)\prime} - p^{(0)} x^{(1)\prime} + p^{(1)} x^{(1)\prime} + x^{(1)} p^{(1)\prime} + x^{(2)} p^{(0)\prime} + 2\lambda\mu z^{(2)}\right) \\
&+ \frac{h}{\lambda}\left[\left(2\mu + \tau^{(0)}_{XX}\right) z^{(1)\prime\prime} + + \tau^{(1)}_{XX} z^{(0)\prime\prime}\right] \\
&- \frac{h^2}{2}\left(p^{(0)} x^{(2)\prime} + 2p^{(1)} x^{(1)\prime} + p^{(2)} x^{(0)\prime} - 2\lambda\mu z^{(3)}\right) \\
&+ \frac{h^2}{2}\left(p^{(0)} x^{(3)\prime} + 2p^{(1)} x^{(2)\prime} + p^{(2)} x^{(1)\prime} + x^{(1)} p^{(2)\prime} + 2x^{(2)} p^{(1)\prime} + x^{(3)} p^{(0)\prime}\right) \\
&+ \frac{h^2}{2\lambda}\left[\left(2\mu + \tau^{(0)}_{XX}\right) z^{(2)\prime\prime} + + 2\tau^{(1)}_{XX} z^{(1)\prime\prime}\right] = q_3^+ - q_3^-.
\end{aligned} \tag{3.19}$$

Note that the higher order terms such as $x^{(n)}$, $z^{(n)}$, $p^{(n)}$ for $n \geq 1$ are expressed in terms of $x^{(0)}$ and $z^{(0)}$ in Appendix.

In Section 3.3, we apply a linear perturbation to this principal solution to investigate stability.

3.3. Linear stability analysis

This section introduces infinitesimally small perturbation of the spatial position vector (3.15) given as

$$x^{(0)} = X + \epsilon U \qquad z^{(0)} = -2h\,(\lambda - 1) + \epsilon W, \tag{3.20}$$

where $0 < \epsilon \ll 1$. In the presence of this small perturbation, the traction q_3^+ at the top surface (Eq. (3.19)) is given by

$$q_3^+(X) = -\alpha_1 \mu\lambda\,[z(x, 2h) - 2h]\,. \tag{3.21}$$

The boundary condition Eq. (3.21) physically represents the case in which the top surface is supported by a flexible Winkler foundation shown in Fig. 2. This flexible support will partially resist lateral deformation during growth and under mechanical loading.

Substituting Eq. (3.20) into the equilibrium Eqs. (3.18) and (3.19), the $\mathcal{O}(\epsilon)$ terms vanish as

$$\beta_{11} U' + \beta_{12} W'' = 0 \tag{3.22}$$

$$\beta_{21} W + \beta_{22} U' + \beta_{23} W'' + \beta_{24} U''' + \beta_{25} W'''' = 0 \tag{3.23}$$

where

$$\beta_{11} = \frac{\left(2 + 6\lambda^2 + \tau^{(0)}_{XX}/\mu\right)\left(1 - h + \frac{h^2}{2}\right)}{\lambda^2} - \frac{h(h-2)\tau^{(1)}_{XX}}{2\mu\lambda}, \tag{3.24}$$

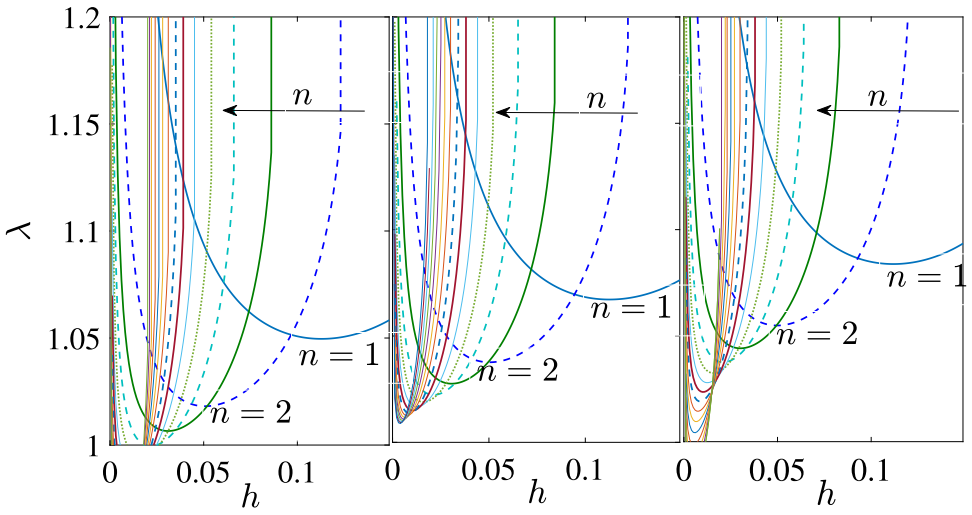

Fig. 3. Critical growth associated with the first 15 instability modes. Left: for initial stress $\tau_{XX}^{(0)} = -0.15\mu$. Middle: in absence of initial stress. Right: for $\tau_{XX}^{(0)} = 0.15\mu$.

$$\beta_{12} = -\left(\frac{4h(1+\lambda^4)}{\lambda} + \frac{\left(1-3h^2\right)\tau_{XX}^{(0)}}{2\mu\lambda}\right) - \frac{3h^2\tau_{XX}^{(1)}}{2\mu}, \tag{3.25}$$

$$\beta_{21} = -\frac{\alpha_1}{2h}, \quad \beta_{22} = \alpha_1\lambda, \tag{3.26}$$

$$\beta_{23} = \frac{2+\tau_{XX}^{(0)}(1-h)/\mu - \left(2+h\alpha_1\right)\lambda^4}{\lambda^2} - \frac{h(h-2)}{2\mu\lambda}\tau_{XX}^{(1)}/\mu, \tag{3.27}$$

$$\beta_{24} = \frac{-12h - 2h^2\alpha_1 - 12h\lambda^4 - 4h^2\alpha_1\lambda^4 + 1.5h^2\tau_{XX}^{(0)}/\mu - 6h\tau_{XX}^{(0)}/\mu + 1.5\tau_{XX}^{(0)}/\mu}{3\lambda} - \frac{3h^2}{2\mu}\tau_{XX}^{(1)}, \tag{3.28}$$

$$\beta_{25} = h^2\left(4 + 4\frac{\lambda^4}{3} + \frac{3\tau_{XX}^{(0)}}{2\mu}\right). \tag{3.29}$$

Substituting Eq. (3.22) into Eq. (3.23), we obtain the following equation:

$$\Psi_0 W + \Psi_2 W'' + \Psi_4 W'''' = 0, \tag{3.30}$$

where $\Psi_0 = \beta_{21}$, $\Psi_2 = \beta_{23} - \beta_{22}\frac{\beta_{12}}{\beta_{11}}$, $\Psi_4 = \beta_{25} - \beta_{24}\frac{\beta_{12}}{\beta_{11}}$. Since both the principal solution (3.15) and the perturbed solution (3.20) satisfy ((3.16), (3.17)), using (3.22), the boundary conditions associated with Eq. (3.30) are obtained as

$$W' = W''' = 0, \quad \text{at } X = -1, 1. \tag{3.31}$$

The eigenvalue problem (3.30) is solved analytically in Section 3.4 to determine various critical modes. In Section 3.5, we use compound matrix method to numerically obtain the critical loads, which we compare with the analytical solution.

3.4. Analytical determination of the critical modes

The general solution to the governing perturbed Eq. (3.30) is given by

$$W = \sum_n A_n \exp \eta_n X. \tag{3.32}$$

To satisfy the boundary condition (3.31) at $X = -1$ and $X = 1$, η_n must be an imaginary number given by

$$\eta_n = \frac{in\pi}{2}, \quad n = 1, 2, 3, \ldots \tag{3.33}$$

Substituting (3.32) into (3.30), we obtain

$$\Psi_0 - \Psi_2\eta_n^2 + \Psi_4\eta_n^4 = 0, \tag{3.34}$$

Since every Ψ_i is a function of λ and $\tau_{XX}^{(0)}$, the critical value of the growth λ is to be determined by solving (3.34) for a given n and $\tau_{XX}^{(0)}$.

Fig. 3 reports the critical growth associated with various modes, and initial stress $\tau_{XX}^{(0)} = -0.15\mu$ (left), $\tau_{XX}^{(0)} = 0$ (middle), and $\tau_{XX}^{(0)} = 0.15\mu$ (right), respectively. We observe that the lower instability-modes are triggered by a compressive initial stress, while a tensile initial stress improves the structural stability for these modes. On the other hand, the higher modes can be destabilized both by the tensile and compressive initial stresses. The destabilizing effect of the compressive initial stress is more clear and distinct.

Fig. 4 further elucidate the instabilities induced by initial stress at the various modes and dimensions. It depicts the variation of critical growth with initial stress for the most critical modes, for different values of h.

For thicker plates, $h = 0.10$, the first mode becomes critical. This mode becomes unstable under a compressive initial stress, and stabilizes in tension, which is expected from an engineering point of view.

The second mode becomes critical for $h = 0.075$. The third mode becomes more critical overtaking the second and the fourth mode for $h = 0.04$. All these modes show the physically interesting behaviour where instabilities are triggered by compression.

For a very thin plate of $h = 0.015$, on the other hand, many higher modes become critical, which are sensitive to both tensile and compressive initial stresses.

For a specified $\tau_{XX}^{(1)}$, i.e., $\frac{\partial \tau_{XX}}{\partial z}\Big|_{z=0}$, the average initial stress is considerably lower for smaller values of h. Consequently, the variation of the initial stress through thickness significantly influences the stability of the thicker plates, not the thinner ones, as illustrated in Fig. 5.

When the magnitude of initial stress is specified at the two boundaries, the through-thickness gradient is higher for smaller h. Fig. 6 describes the cases for which the initial stress vanishes on the lower surface and is specified as 0.15μ (or -0.15μ) on the upper surface. In these cases, $\tau_{XX}^{(0)} = 0$ and $\tau_{XX}^{(1)} = 0.15\mu/h$ (left) or $\tau_{XX}^{(1)} = -0.15\mu/h$ (right). We observe that it is impossible to ignore the influence on thinner plates; a tensile initial stress stabilizes the structure for all h, whereas a compressive initial stress leads to instability.

In Section 3.5, we apply the compound matrix method to determine the minimum critical growth in the presence of different initial stresses, and compare it with the present results.

3.5. Determining the critical growth using compound matrix method

It is noted that in engineering design, we very often do not require the complete details of every mode. As explained in Fig. 4, determining the most critical mode is usually the primary interest. In this section,

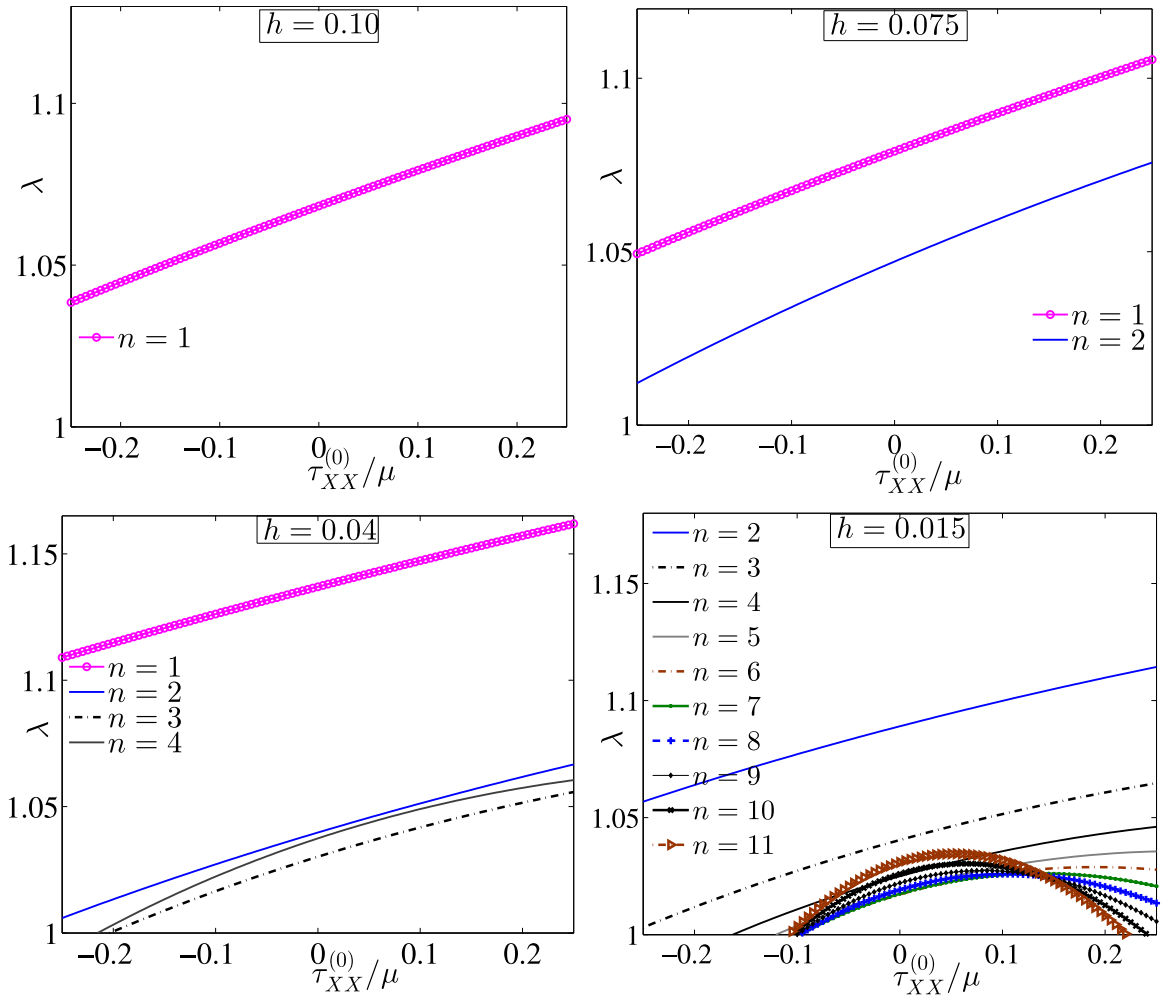

Fig. 4. The influence of initial stress on the most critical modes for different thicknesses. Top right: $h = 0.10$; the most critical mode: $n = 1$. Top left: $h = 0.075$; the most critical mode: $n = 2$. Bottom left: $h = 0.04$; the most critical mode: $n = 3$. Bottom right: $h = 0.015$.

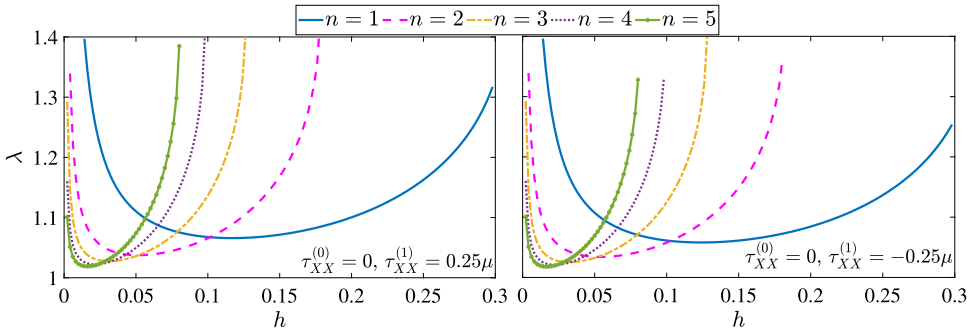

Fig. 5. The variation of critical growth-rate with thickness, for $\tau^{(0)}_{XX} = 0$ while $\tau^{(1)}_{XX} = 0.25\mu$ (left) and $\tau^{(1)}_{XX} = -0.25\mu$ (right). An initial tensile stress induces stability for thicker plates.

we numerically determine the critical values of growth at different initial stress, which is compared with our analytical results. The present results precisely describe the collective influence of initial stress at the onset of instability.

The governing fourth-order Eq. (3.30) can be equivalently expressed in the following set of first order equations,

$$\mathcal{A}\mathcal{W} = \mathcal{W}', \tag{3.35}$$

where

$$\mathcal{A} = \begin{bmatrix} 0 & 1 & 0 & 0 \\ 0 & 0 & 1 & 0 \\ 0 & 0 & 0 & 1 \\ -\frac{\Psi_0}{\Psi_4} & 0 & -\frac{\Psi_2}{\Psi_4} & 0 \end{bmatrix} \qquad \mathcal{W} = \begin{Bmatrix} W \\ W' \\ W'' \\ W''' \end{Bmatrix} \tag{3.36}$$

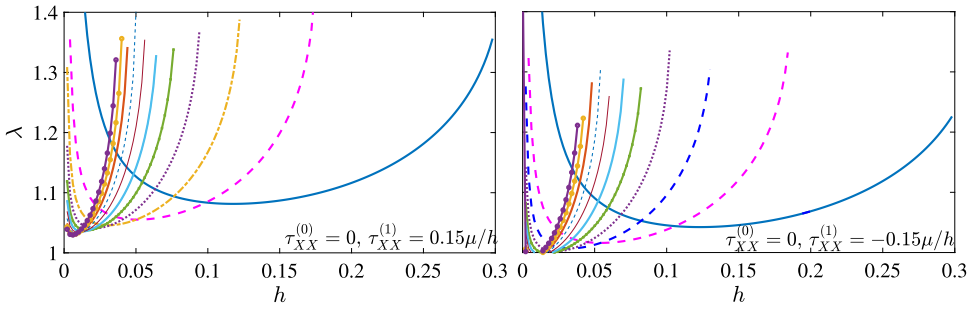

Fig. 6. The critical growth rate when the initial stress is vanishes at the lower surface, is specified at the upper surface as 0.15μ (left) and -0.15μ (right); a linear variation of initial stress is considered.

Similarly, the boundary conditions (3.31) can be represented by

$$\mathcal{B}\mathcal{W}\Big|_{X=-1} = 0 \qquad C\mathcal{W}\Big|_{X=1} = 0 \tag{3.37}$$

where

$$\mathcal{B} = C = \begin{bmatrix} 0 & 1 & 0 & 0 \\ 0 & 0 & 0 & 1 \end{bmatrix} \tag{3.38}$$

We use compound matrix method to transform the above boundary value problem with unknown critical growth (λ_{cr}) as an initial (eigen-)value problem.

It should be noted that the boundary condition (3.37a) is satisfied by an arbitrary linear combinations following boundary values of the vector function $\mathcal{W}$:

$$\mathcal{W}^{(1)}(-1) = \begin{Bmatrix} 1 \\ 0 \\ 0 \\ 0 \end{Bmatrix} \qquad \mathcal{W}^{(2)}(-1) = \begin{Bmatrix} 0 \\ 0 \\ 1 \\ 0 \end{Bmatrix} \tag{3.39}$$

The displacement vector $\mathcal{W}(X)$ can be expressed as

$$\mathcal{W}(X) = \mathfrak{W}\boldsymbol{k} \tag{3.40}$$

where

$$\mathfrak{W}(X) = \begin{bmatrix} \mathcal{W}_1^{(1)}(X) & \mathcal{W}_1^{(2)}(X) \\ \mathcal{W}_2^{(1)}(X) & \mathcal{W}_2^{(2)}(X) \\ \mathcal{W}_3^{(1)}(X) & \mathcal{W}_3^{(2)}(X) \\ \mathcal{W}_4^{(1)}(X) & \mathcal{W}_4^{(2)}(X) \end{bmatrix}, \tag{3.41}$$

and

$$\boldsymbol{k} = \begin{Bmatrix} k_1 \\ k_2 \end{Bmatrix}. \tag{3.42}$$

The boundary condition (3.37) is expressed as

$$C\mathfrak{W}(1)\,\boldsymbol{k} = 0 \tag{3.43}$$

In compound matrix method, new vector variables $\kappa_{i,j}$ are formed using the following minors of the solution matrix

$$\kappa_{i,j}(X) = \begin{vmatrix} \mathcal{W}_i^{(1)}(X) & \mathcal{W}_j^{(2)}(X) \\ \mathcal{W}_j^{(1)}(X) & \mathcal{W}_j^{(2)}(X) \end{vmatrix}, \tag{3.44}$$

For simplicity, we consider

$$\begin{aligned} &\gamma_1 = \kappa_{1,2} && \gamma_2 = \kappa_{1,3} && \gamma_3 = \kappa_{1,4} \\ &\gamma_4 = \kappa_{2,3} && \gamma_5 = \kappa_{2,4} && \gamma_6 = \kappa_{3,4} \end{aligned} \tag{3.45}$$

The set of first order Eqs. (3.35) are expressed in terms of $\boldsymbol{\gamma}$ as

$$\mathfrak{A}\boldsymbol{\gamma} = \boldsymbol{\gamma}' \tag{3.46}$$

where

$$\mathfrak{A} = \begin{bmatrix} 0 & 1 & 0 & 0 & 0 & 0 \\ 0 & 0 & 1 & 1 & 0 & 0 \\ 0 & -\frac{\Psi_2}{\Psi_4} & 0 & 0 & 1 & 0 \\ 0 & 0 & 0 & 0 & 1 & 0 \\ \frac{\Psi_0}{\Psi_4} & 0 & 0 & -\frac{\Psi_2}{\Psi_4} & 0 & 1 \\ 0 & \frac{\Psi_0}{\Psi_4} & 0 & 0 & 0 & 0 \end{bmatrix} \tag{3.47}$$

Similarly, the boundary condition (3.39) can be expressed in terms of the new variables as

$$\boldsymbol{\gamma}(-1) = \begin{Bmatrix} \gamma_1 \\ \gamma_2 \\ \gamma_3 \\ \gamma_4 \\ \gamma_5 \\ \gamma_6 \end{Bmatrix} = \begin{Bmatrix} 0 \\ 1 \\ 0 \\ 0 \\ 0 \\ 0 \end{Bmatrix} \tag{3.48}$$

The boundary condition (3.37b) and (3.43) at $X = 1$ is satisfied when

$$\det\left[C\mathfrak{W}(1)\right] = 0. \tag{3.49}$$

The present compound matrix method solves the system of Eq. (3.46) using the initial condition (3.48). The critical value of growth λ_{cr} satisfies the boundary condition (3.49). Fig. 7 reports the critical value of growth λ for various thickness h and magnitude of initial stress $\tau_{XX}^{(0)}$. As also observed in Section 3.4, a compressive initial stress $\tau_{XX}^{(0)}$ hastens the wrinkling/ instability. For e.g., for $\tau_{XX}^{(0)} = -0.20\mu$, instability takes place in absence of growth for $h < 0.04$.

A tensile initial stress, on the other hand, stabilizes the rectangular plate, for thicker plates. However, for smaller plate thicknesses, where higher modes of instabilities are activated, (see Fig. 3 as well), both tensile and compressive initial stresses can hasten wrinkling.

We compare the analytical results (of Fig. 3, Section 3.4) with that of compound matrix method (Fig. 7) in Fig. 8 which shows an excellent agreement.

4. Conclusion

Both growth and residual stresses play a critical role in inducing wrinkling in thin, soft biological structures. This paper introduces a consistent theoretical framework for initially stressed plates undergoing growth, performing both analytical and numerical stability analyses. For the numerical approach, we develop and implement the compound matrix method (CMM) tailored to this novel theory, effectively capturing the critical growth threshold for wrinkling onset. The analytical

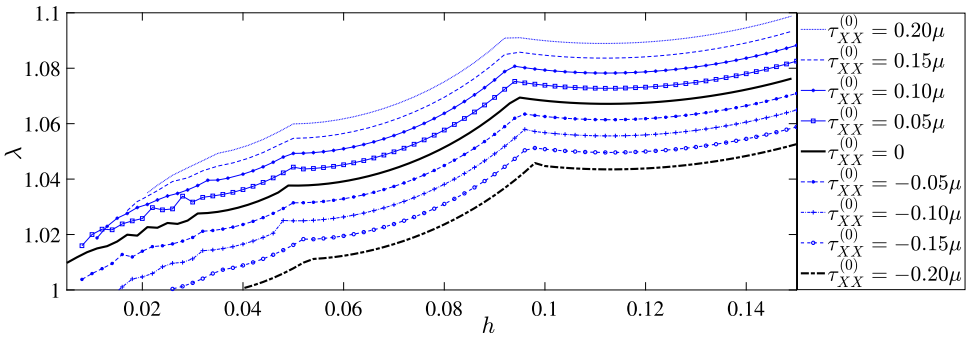

Fig. 7. The lowest critical growth λ for instability. A tensile initial stress stabilizes wrinkling modes of instability, which a compressive initial stress further destabilizes.

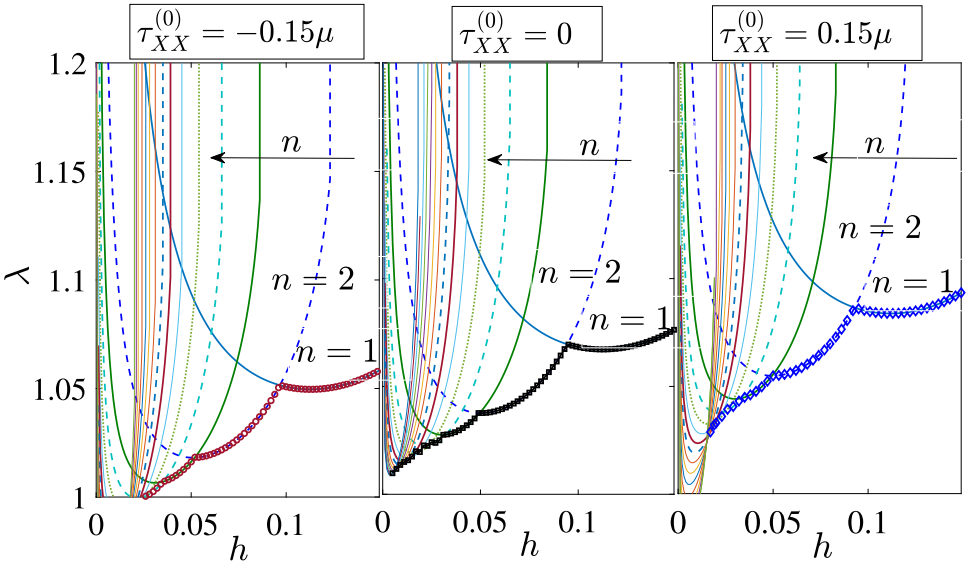

Fig. 8. Comparing the analytically determined critical growth with the results of the compound matrix method. Thin curves show the analytically determined critical growth associated with the first 15 instability modes. The larger markers represent the numerical results.

solution, in contrast, provides distinct insights into individual instability modes. Both methods align well, demonstrating the validity of the approach. The current plate theory and the CMM computational framework can be expanded to tackle more complex boundary value problems (BVPs).

Our stability analysis, applied to a plate on a Winkler foundation, reveals notable results: lower instability modes, which dominate in thicker or moderately thick plates, are stabilized under tensile axial stress, whereas compressive axial stress destabilizes these modes. Conversely, higher instability modes, critical in very thin plates, are destabilized by both tensile and compressive initial stresses, with compressive stress exerting a more pronounced influence on instability onset. The results, presented through various plots, show critical growth variations as functions of thickness and initial stress. These findings align with established stability results for Couette flow over initially stressed solids (Mukherjee and Giribabu, 2021).

Since residual stress is a natural consequence of growth, repair, and remodelling in thin structures, like skin, this plate theory has broad applicability in biomechanics and engineering. For instance, interfacial growth during wound healing introduces residual stress that can lead to wrinkling (Swain and Gupta, 2015, 2016), an effect that can be analysed without knowing the original, stress-free configuration. This theory thus provides a robust tool for studying wrinkling and instability in a range of biomechanical and engineering contexts.

CRediT authorship contribution statement

Soumya Mukherjee: Writing – original draft, Visualization, Software, Methodology, Investigation, Formal analysis, Data curation, Conceptualization. **Prashant Saxena:** Writing – review & editing, Supervision, Methodology, Funding acquisition, Formal analysis, Conceptualization.

Declaration of competing interest

The authors declare that they do not have any conflict of interest.

Acknowledgements

Soumya Mukherjee acknowledges Faculty Seed Grand, Indian Institute of Technology Palakkad. Prashant Saxena acknowledges the financial support of the Engineering and Physical Sciences Research Council via project no. EP/V030833/1.

Appendix. Determining the higher order terms of spatial position and Lagrange multiplier

In this section, we express the higher order terms $x^{(1)}$, $x^{(2)}$, $x^{(3)}$, $z^{(1)}$, $z^{(2)}$, $z^{(3)}$, in the spatial position, and the Lagrange multipliers $p^{(0)}$, $p^{(1)}$, $p^{(2)}$, $p^{(3)}$. The method described in Section 3 is used, where we extend the work of Wang et al. (2018b) on stress-free plates.

The expressions for $x^{(1)}$, $z^{(1)}$, and $p^{(0)}$ do not depend on initial stress $\boldsymbol{\tau}$, for the simple model we have used in this paper. For traction-free bottom surface ($q^- = 0$), these quantities are determined from the boundary condition (2.27), rewritten as

$$2\lambda\mu x^{(1)} + p^{(0)} z^{(0)'} = 0, \tag{A.1}$$

$$2\lambda\mu z^{(1)} - p^{(0)} x^{(0)'} = 0, \tag{A.2}$$

and Eq. (3.9), rewritten as

$$\det \boldsymbol{F}_0 = \det \boldsymbol{G}_0 = \lambda. \tag{A.3}$$

Solving the above equations, the quantities $x^{(1)}$, $z^{(1)}$, and $p^{(0)}$ are expressed in terms of $x^{(0)}$ and $z^{(0)}$ as

$$x^{(1)} = \frac{-\lambda \left(z^{(0)'}\right)}{\left(x^{(0)'}\right)^2 + \left(z^{(0)'}\right)^2} \tag{A.4}$$

$$z^{(1)} = \frac{\lambda \left(x^{(0)'}\right)}{\left(x^{(0)'}\right)^2 + \left(z^{(0)'}\right)^2}. \tag{A.5}$$

$$p^{(0)} = \frac{2\mu\lambda^2}{\left(x^{(0)'}\right)^2 + \left(z^{(0)'}\right)^2} \tag{A.6}$$

The higher order terms, however, depend on the initial stress $\tau^{(0)}_{XX}$. For e.g., $x^{(2)}$, $z^{(2)}$, and $p^{(1)}$ are expressed in terms of $x^{(0)}$, $z^{(0)}$, $x^{(1)}$ (Eq. (A.4)), and $z^{(1)}$ (Eq. (A.5)), $p^{(0)}$ (Eq. (A.6)) as follows,

$$\begin{aligned} x^{(2)} = \frac{-1}{2\mu\lambda^2\left[\left(\left(x^{(0)'}\right)^2 + \left(z^{(0)'}\right)^2\right)\right]} \Big[& \left(2\mu + \tau^{(0)}_{XX}\right)\left(x^{(0)'}\right)^2 x^{(0)''} \\ & - \lambda z^{(1)} p^{(0)'}\left(x^{(0)'}\right)^2 + 2\mu\lambda^2 x^{(1)}\left(x^{(0)'}\right)^2 + \left(2\mu + \tau^{(0)}_{XX}\right) x^{(0)'} z^{(0)'} z^{(0)''} \\ & + \lambda x^{(1)} p^{(0)'} x^{(0)'} z^{(0)'} + 2\mu\lambda^2 z^{(1)} x^{(0)'} z^{(0)'} + 2\mu\lambda^2 x^{(1)} z^{(0)'} z^{(1)'} \\ & - 2\mu\lambda^2 z^{(1)} x^{(1)'} z^{(0)'} \Big] \end{aligned} \tag{A.7}$$

$$\begin{aligned} z^{(2)} = \frac{-1}{2\mu\lambda^2\left[\left(\left(x^{(0)'}\right)^2 + \left(z^{(0)'}\right)^2\right)\right]} \Big[& \left(2\mu + \tau^{(0)}_{XX}\right)\left(z^{(0)'}\right)^2 z^{(0)''} \\ & + \lambda x^{(1)} p^{(0)'}\left(z^{(0)'}\right)^2 + 2\mu\lambda^2 z^{(1)}\left(z^{(0)'}\right)^2 + \left(2\mu + \tau^{(0)}_{XX}\right) x^{(0)'} z^{(0)'} x^{(0)''} \\ & - \lambda z^{(1)} p^{(0)'} x^{(0)'} z^{(0)'} + 2\mu\lambda^2 x^{(1)} x^{(0)'} z^{(0)'} \\ & - 2\mu\lambda^2 x^{(1)} x^{(0)'} z^{(1)'} + 2\mu\lambda^2 z^{(1)} x^{(0)'} x^{(1)'} \Big] \end{aligned} \tag{A.8}$$

$$\begin{aligned} p^{(1)} = \frac{1}{\lambda\left[\left(x^{(0)'}\right)^2 + \left(z^{(0)'}\right)^2\right]} \Big[& \left(2\mu + \tau^{(0)}_{XX}\right)\left(x^{(0)'} z^{(0)''} - z^{(0)'} x^{(0)''}\right) \\ & - \lambda p^{(0)}\left[\left(x^{(0)'}\right)^2 + \left(z^{(0)'}\right)^2\right] + \lambda p^{(0)'}\left(x^{(1)} x^{(0)'} + z^{(1)} z^{(0)'}\right) \\ & - 2\mu\lambda^2 x^{(1)} z^{(0)'} + 2\mu\lambda^2 z^{(1)} x^{(0)'} + 2\mu\lambda^2 x^{(1)} z^{(1)'} - 2\mu\lambda^2 z^{(1)} x^{(1)'} \Big] \end{aligned} \tag{A.9}$$

The terms $x^{(3)}$, $z^{(3)}$, and $p^{(2)}$ are expressed in terms of the above quantities as follows,

$$\begin{aligned} x^{(3)} = \frac{-1}{2\mu\lambda^2\left[\left(x^{(0)'}\right)^2 + \left(z^{(0)'}\right)^2\right]} \Big[& \left(2\mu + \tau^{(0)}_{XX}\right)\left(x^{(0)'}\right)^2 x^{(1)''} \\ & + \tau^{(1)}_{XX}\left(x^{(0)'}\right)^2 x^{(0)''} + \tau^{(1)}_{XX} x^{(0)'} z^{(0)'} z^{(0)''} + \lambda p^{(0)}\left(x^{(0)'}\right)^2 z^{(1)'} \\ & + \lambda p^{(1)}\left(x^{(0)'}\right)^2 z^{(1)'} - \lambda z^{(1)} p^{(1)'}\left(x^{(0)'}\right)^2 - \lambda z^{(2)} p^{(0)'}\left(x^{(0)'}\right)^2 \\ & + 2\lambda^2\mu x^{(2)}\left(x^{(0)'}\right)^2 + \left(2\mu + \tau^{(0)}_{XX}\right) x^{(0)'} z^{(0)'} z^{(1)''} - \lambda p^{(0)} x^{(0)'} x^{(1)'} z^{(0)'} \\ & - \lambda p^{(1)} x^{(0)'} x^{(1)'} z^{(0)'} + \lambda x^{(1)} p^{(1)'} x^{(0)'} z^{(0)'} + \lambda x^{(2)} p^{(0)'} x^{(0)'} z^{(0)'} \\ & + 2\lambda^2\mu z^{(2)} x^{(0)'} z^{(0)'} + 2\lambda^2\mu z^{(1)} x^{(0)'} z^{(2)'} + 4\lambda^2\mu z^{(2)} x^{(0)'} z^{(1)'} \\ & - 2\lambda^2\mu z^{(1)} x^{(2)'} z^{(0)'} - 4\lambda^2\mu z^{(2)} x^{(1)'} z^{(0)'} \Big], \end{aligned} \tag{A.10}$$

$$\begin{aligned} z^{(3)} = \frac{-1}{2\mu\lambda^2\left[\left(x^{(0)'}\right)^2 + \left(z^{(0)'}\right)^2\right]} \Big[& \left(2\mu + \tau^{(0)}_{XX}\right)\left(z^{(0)'}\right)^2 z^{(1)''} \\ & + \tau^{(1)}_{XX}\left(z^{(0)'}\right)^2 z^{(0)''} + \tau^{(1)}_{XX} x^{(0)'} z^{(0)'} z^{(0)''} - \lambda p^{(0)} x^{(1)'}\left(z^{(0)'}\right)^2 \\ & - \lambda p^{(1)} x^{(1)'}\left(z^{(0)'}\right)^2 + \lambda x^{(1)} p^{(1)'}\left(z^{(0)'}\right)^2 + \lambda x^{(2)} p^{(0)'}\left(z^{(0)'}\right)^2 \\ & + 2\lambda^2\mu z^{(2)}\left(z^{(0)'}\right)^2 + 2\left(2\mu + \tau^{(0)}_{XX}\right) x^{(0)'} z^{(0)'} x^{(1)''} + \lambda p^{(0)} x^{(0)'} z^{(0)'} z^{(1)'} \\ & + \lambda p^{(1)} x^{(0)'} z^{(0)'} z^{(1)'} - \lambda z^{(1)} p^{(1)'} x^{(0)'} z^{(0)'} - \lambda z^{(2)} p^{(0)'} x^{(0)'} z^{(0)'} \\ & + 2\lambda^2\mu x^{(2)} x^{(0)'} z^{(0)'} - 2\lambda^2\mu x^{(1)} x^{(0)'} z^{(2)'} - 4\lambda^2\mu x^{(2)} x^{(0)'} z^{(1)'} \\ & + 2\lambda^2\mu z^{(1)} x^{(0)'} x^{(2)'} + 4\lambda^2\mu z^{(2)} x^{(0)'} x^{(1)'} \Big], \end{aligned} \tag{A.11}$$

$$\begin{aligned} p^{(2)} = \frac{-1}{\lambda\left[\left(x^{(0)'}\right)^2 + \left(z^{(0)'}\right)^2\right]} \Big[& \left(2\mu + \tau^{(0)}_{XX}\right) z^{(0)'} x^{(1)''} \\ & - \left(2\mu + \tau^{(0)}_{XX}\right) x^{(0)'} z^{(1)''} - \tau^{(1)}_{XX}\left(x^{(0)'} z^{(0)''} - x^{(0)''} z^{(0)'}\right) \\ & + \lambda p^{(1)}\left(x^{(0)'}\right)^2 + \lambda p^{(1)}\left(z^{(0)'}\right)^2 + \lambda p^{(0)} x^{(0)'} x^{(1)'} + \lambda p^{(1)} x^{(0)'} x^{(1)'} \\ & - \lambda x^{(1)} p^{(1)'} x^{(0)'} - \lambda x^{(2)} p^{(0)'} x^{(0)'} + \lambda p^{(0)} z^{(0)'} z^{(1)'} + \lambda p^{(1)} z^{(0)'} z^{(1)'} \\ & - \lambda z^{(1)} p^{(1)'} z^{(0)'} - \lambda z^{(2)} p^{(0)'} z^{(0)'} + 2\lambda^2\mu x^{(2)} z^{(0)'} - 2\lambda^2\mu z^{(2)} x^{(0)'} \\ & - 2\lambda^2\mu x^{(1)} z^{(2)'} - 4\lambda^2\mu x^{(2)} z^{(1)'} + 2\lambda^2\mu z^{(1)} x^{(2)'} + 4\lambda^2\mu z^{(2)} x^{(1)'} \Big]. \end{aligned} \tag{A.12}$$

Data availability

No data was used for the research described in the article.

References

Dai, H.-H., Song, Z., 2014. On a consistent finite-strain plate theory based on three-dimensional energy principle. Proc. R. Soc. A: Math. Phys. Eng. Sci. 470 (2171), 20140494.

Dorfmann, A., Haughton, D.M., 2006. Stability and bifurcation of compressed elastic cylindrical tubes. Internat. J. Engrg. Sci. 44 (18–19), 1353–1365.

Fu, Y., 2007. Linear and nonlinear wave propagation in coated or uncoated elastic half-spaces. Waves Nonlinear Pre- Stress. Mater. 103–127.

Fu, Y., Kaplunov, J., Prikazchikov, D., 2020. Reduced model for the surface dynamics of a generally anisotropic elastic half-space. Proc. R. Soc. A 476 (2234), 20190590.

Gower, A.L., Ciarletta, P., Destrade, M., 2015. Initial stress symmetry and its applications in elasticity. Proc. R. Soc. A: Math. Phys. Eng. Sci. 471 (2183), 20150448.

Hilgers, M.G., Pipkin, A.C., 1992a. Bending energy of highly elastic membranes. Quart. Appl. Math. 50.2, 389–400.

Hilgers, M.G., Pipkin, A.C., 1992b. Elastic sheets with bending stiffness. Quart. J. Mech. Appl. Math. 45.1, 57–75.

Hoger, A., 1985. On the residual stress possible in an elastic body with material symmetry. Arch. Ration. Mech. Anal. 88 (3), 271–289.

Johnson, B.E., Hoger, A., 1993. The dependence of the elasticity tensor on residual stress. J. Elasticity 33 (2), 145–165.

Johnson, B.E., Hoger, A., 1995. The use of a virtual configuration in formulating constitutive equations for residually stressed elastic materials. J. Elasticity 41 (3), 177–215.

Kienzler, R., 2002. On consistent plate theories. Arch. Appl. Mech. 72 (4–5), 229–247. http://dx.doi.org/10.1007/s00419-002-0220-2, Cited by: 76.

Lewicka, M., Mahadevan, L., Pakzad, M.R., 2011. The Föppl-von Kármán equations for plates with incompatible strains. Proc. R. Soc. A: Math. Phys. Eng. Sci. 467 (2126), 402–426.

Liang, H., Mahadevan, L., 2009. The shape of a long leaf. Proc. Natl. Acad. Sci. 106 (52), 22049–22054.

Liang, H., Mahadevan, L., 2011. Growth, geometry, and mechanics of a blooming lily. Proc. Natl. Acad. Sci. 108 (14), 5516–5521.

Love, A.E.H., 2013. A Treatise on the Mathematical Theory of Elasticity. Cambridge University Press.

Mehta, S., Raju, G., Kumar, S., Saxena, P., 2022a. Instabilities in a compressible hyperelastic cylindrical channel under internal pressure and external constraints. Int. J. Non-Linear Mech. 144, 104031.

Mehta, S., Raju, G., Saxena, P., 2021. Growth induced instabilities in a circular hyperelastic plate. Int. J. Solids Struct. 226, 111026.

Mehta, S., Raju, G., Saxena, P., 2022b. Wrinkling as a mechanical instability in growing annular hyperelastic plates. Int. J. Mech. Sci. 229, 107481.
Merodio, J., Ogden, R.W., 2016. Extension, inflation and torsion of a residually stressed circular cylindrical tube. Contin. Mech. Thermodyn. 28 (1–2), 157–174.
Merodio, J., Ogden, R.W., Rodríguez, J., 2013. The influence of residual stress on finite deformation elastic response. Int. J. Non-Linear Mech. 56, 43–49.
Mukherjee, S., 2022a. Constitutive relation, limited stretchability, and stability of residually stressed gent materials. Mech. Res. Commun. 120, 103850.
Mukherjee, S., 2022b. Influence of residual stress in failure of soft materials. Mech. Res. Commun. 123, 103903.
Mukherjee, S., 2024. Representing implicit elasticity from a residually stressed reference. Internat. J. Engrg. Sci. 201, 104079.
Mukherjee, S., Destrade, M., Gower, A.L., 2022. Representing the stress and strain energy of elastic solids with initial stress and transverse texture anisotropy. Proc. R. Soc. A 478 (2266), 20220255.
Mukherjee, S., Giribabu, D., 2021. Stability of plane couette flow past an initially stressed solid. Internat. J. Engrg. Sci. 169, 103572.
Mukherjee, S., Mandal, A.K., 2021. Static and dynamic characteristics of a compound sphere using initial stress reference independence. Int. J. Non-Linear Mech. 128, 103617.
Mukherjee, S., Ravindran, P., 2024. Representation of stress and free energy for a viscoelastic body from a stressed reference. J. Mech. Phys. Solids 184, 105544.
Nam, N.T., Merodio, J., Ogden, R.W., Vinh, P.C., 2016. The effect of initial stress on the propagation of surface waves in a layered half-space. Int. J. Solids Struct. 88, 88–100.
Ng, B.S., Reid, W.H., 1980. On the numerical solution of the orr-sommerfeld problem: asymptotic initial conditions for shooting methods. J. Comput. Phys. 38 (3), 275–293.
Ng, B.S., Reid, W.H., 1985. The compound matrix method for ordinary differential systems. J. Comput. Phys. 58 (2), 209–228.
Pidge, P.A., Kumar, H., 2020. Additive manufacturing: A review on 3 d printing of metals and study of residual stress, buckling load capacity of strut members. Mater. Today: Proc. 21, 1689–1694.
Quelho de Macedo, R., Ferreira, R.T.L., Jayachandran, K., 2019. Determination of mechanical properties of FFF 3D printed material by assessing void volume fraction, cooling rate and residual thermal stresses. Rapid Prototyp. J. 25 (10), 1661–1683.
Rajagopal, K.R., Wineman, A., 2024. Residual stress and material symmetry. Internat. J. Engrg. Sci. 197, 104013.
Reddy, N.H., Saxena, P., 2018. Instabilities in the axisymmetric magnetoelastic deformation of a cylindrical membrane. Int. J. Solids Struct. 136, 203–219.
Salerno, G., Bennett, C., Sun, W., Becker, A., Palumbo, N., Kelleher, J., Zhang, S.Y., 2018. On the interaction between welding residual stresses: a numerical and experimental investigation. Int. J. Mech. Sci. 144, 654–667.
Saravanan, U., 2008. Representation for stress from a stressed reference configuration. Internat. J. Engrg. Sci. 46 (11), 1063–1076.
Saravanan, U., 2011. On large elastic deformation of prestressed right circular annular cylinders. Int. J. Non-Linear Mech. 46 (1), 96–113.
Shams, M., Destrade, M., Ogden, R.W., 2011. Initial stresses in elastic solids: constitutive laws and acoustoelasticity. Wave Motion 48 (7), 552–567.
Steigmann, D.J., 2007. Thin-plate theory for large elastic deformations. Int. J. Non-Linear Mech. 42 (2), 233–240.
Steigmann, D.J., 2013. Koiter's shell theory from the perspective of three-dimensional nonlinear elasticity. J. Elasticity 111, 91–107.
Sun, L., Ren, X., He, J., Zhang, Z., 2021. A bead sequence-driven deposition pattern evaluation criterion for lowering residual stresses in additive manufacturing. Addit. Manuf. (ISSN: 2214-8604) 48, 102424. http://dx.doi.org/10.1016/j.addma.2021.102424.
Swain, D., Gupta, A., 2015. Interfacial growth during closure of a cutaneous wound: stress generation and wrinkle formation. Soft Matter 11 (32), 6499–6508.
Swain, D., Gupta, A., 2016. Mechanics of cutaneous wound rupture. J. Biomech. 49 (15), 3722–3730.
Wang, F., Mao, K., Li, B., 2018a. Prediction of residual stress fields from surface stress measurements. Int. J. Mech. Sci. 140, 68–82.
Wang, J., Song, Z., Dai, H.-H., 2016. On a consistent finite-strain plate theory for incompressible hyperelastic materials. Int. J. Solids Struct. 78, 101–109.
Wang, F.-F., Steigmann, D.J., Dai, H.-H., 2019. On a uniformly-valid asymptotic plate theory. Int. J. Non-Linear Mech. 112, 117–125.
Wang, J., Steigmann, D., Wang, F.-F., Dai, H.-H., 2018b. On a consistent finite-strain plate theory of growth. J. Mech. Phys. Solids 111, 184–214.